Geophysical Journal International

Geophys. J. Int. (2024) **237,** 1093–1108
Advance Access publication 2024 March 8
GJI Geodynamics and Tectonics

https://doi.org/10.1093/gji/ggae096

Increasing accuracy of 3-D geomechanical-numerical models

Moritz O. Ziegler [1,2] and Oliver Heidbach[2,3]

[1] *Professorship of Geothermal Technologies, Technical University of Munich, Arcisstraße* 21, 80333 *Munich, Germany. E-mail: mziegler@gfz-potsdam.de*
[2] *Helmholtz Centre Potsdam GFZ German Research Centre for Geosciences, Telegrafenberg,* 14473 *Potsdam, Germany*
[3] *Institute for Applied Geosciences, Technical University Berlin, Ernst-Reuter-Platz 1,* 10587 *Berlin, Germany*

Accepted 2024 March 7. Received 2024 February 29; in original form 2023 December 12

SUMMARY

The current crustal stress field is of key importance to understand geodynamic processes and to assess stability aspects during subsurface usage. To provide a 3-D continuous description of the stress state, linear elastic forward geomechanical-numerical models are used. These models solve the equilibrium of forces between gravitational volume forces and surfaces forces imposed mainly by plate tectonics. The latter are responsible for the horizontal stress anisotropy and impose the inverse problem to estimate horizontal displacement boundary conditions that provide a fit best to horizontal stress magnitude data within the model volume. However, horizontal stress magnitude data have high uncertainties and they are sparse, clustered and not necessarily representative for a larger rock volume. Even when Bayesian statistics are incorporated and additional stress information such as borehole failure observations or formation integrity test are used to further constrain the solution space, this approach may result in a low accuracy of the model results, that is the result is not correct. Here, we present an alternative approach that removes the dependence of the solution space based on stress magnitude data to avoid potential low accuracy. Initially, a solution space that contains all stress states that are physically reasonable is defined. Stress magnitude data and the additional stress information are then used in a Bayesian framework to evaluate which solutions are more likely than others. We first show and validate our approach with a generic truth model and then apply it to a case study of the Molasse foreland basin of the Alps in Southern Germany. The results show that the model's ability to predict a reliable stress state is increasing while the number of likely solutions may also increase, and that outlier of stress magnitude data can be identified. This alternative approach results in a substantial increase in computational speed as we perform most of the calculations analytically.

Key words: Numerical modelling; Statistical methods; Geomechanics; Mechanics, theory and modelling; Uncertainties.

1 INTRODUCTION

The contemporary stress field in the Earth crust is one of the key field quantities that control geodynamic processes. Deformation due to tectonic forces constantly increase the stored elastic energy until a critical value is reached and failure occurs along faults (Ziebarth *et al*. 2020; Kanamori 1994). Release of stored elastic energy is also observed during the anthropogenic utilization of the subsurface (Segall & Fitzgerald 1998; Ziegler *et al*. 2015; van Wees *et al*. 2018) and expressed, for example as brittle failure of boreholes (Plumb & Hickman 1985; Schmitt *et al*. 2012), caverns and tunnels (Brady & Brown 2006) or induced seismic events (Rutqvist *et al*. 2008; Ellsworth 2013; Altmann *et al*. 2014; Müller *et al*. 2018; Gaucher *et al*. 2015; Schoenball *et al*. 2018). Thus, to develop mitigation strategies for induced hazard it is important to understand the undisturbed 3-D *in situ* stress state as it describes the distance to failure (e.g. Müller *et al*. 2018; Meyer *et al*. 2023).

To obtain a continuous description of the 3-D stress tensor in a given rock volume at reservoir scale, geomechanical-numerical models are used that solve the partial differential equation of the equilibrium of forces

$$\frac{\partial \sigma_{ij}}{\partial x_i} + \rho X_j = 0. \quad (1)$$

The second term describes the gravitational volume forces controlled by the density distribution ρ and the first term are the surface forces that result from plate tectonics expressed by the changes of the stress tensor σ_{ij} with respect to location x_i. Assuming linear elasticity the constitutive equation between stress σ_{ij} and strain ε_{ij} is

$$\sigma_{ij} = \lambda \varepsilon_{kk} \delta_{ij} + 2\mu \varepsilon'_{ij}, \quad (2)$$

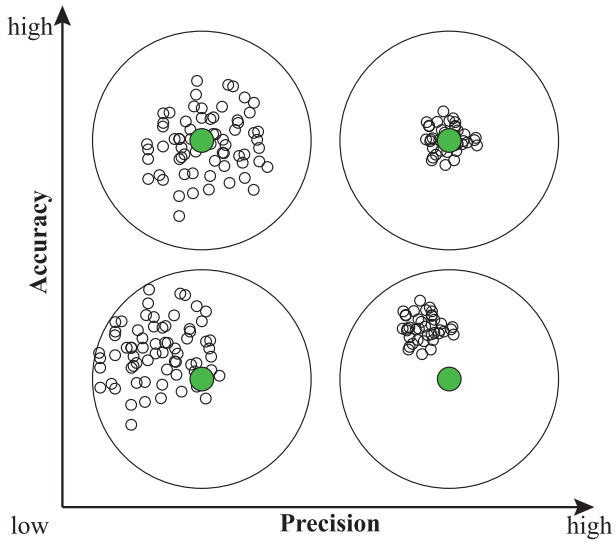

Figure 1. Sketch to visualize the terms accuracy (*y*-axis) and precision (*x*-axis). Green point is the real but unknown solution. White circles show the distribution of a large number of model scenarios. Thus, a low accuracy results in a non-reliable prediction of the model results.

where $\varepsilon^{'}_{ij}$ is the deviatoric part of the strain tensor

$$\varepsilon_{ij} = \left(\frac{\partial u_i}{\partial x_j} + \frac{\partial u_j}{\partial x_i}\right) \tag{3}$$

and λ and μ are the two Lamé parameters that can be translated into the elastic parameter ν and E, the Poisson's ratio and the Young's modulus, respectively (Jaeger *et al.* 2007). Inserting eqs (2) and (3) into the equation of the equilibrium of forces (eq. 1) the resulting partial differential equation is of second order with displacement u as the field variable (Jaeger *et al.* 2007).

This results in the inverse problem to estimate reasonable horizontal displacement boundary conditions that provide a best fit with respect to stress magnitude data within the model volume (Reiter & Heidbach 2014; Ziegler *et al.* 2016; Rajabi *et al.* 2017; Roche & Van Der Baan 2017). In the following we assume that the vertical stress S_V is a principal stress which implies that the minimum and maximum horizontal stresses S_{hmin} and S_{Hmax}, respectively are principal stresses as well. This is true for our generic model and a reasonable assumption for the case study presented in Section 4.5.

A key problem of stress magnitude data is that they often have high uncertainties and that they are sparse and clustered. Furthermore, *in situ* S_{hmin} measurements using microhydraulic fracturing (MHF) tests (Haimson & Cornet 2003; Schmitt *et al.* 2012; Desroches *et al.* 2021) and dry sleeve re-opening tests to derive the maximum horizontal stress S_{Hmax} (Amadei & Stephansson 1997; Desroches *et al.* 2021) sample the rock volume on a meter scale and thus have the potential to be not representative for a larger rock volume (Ljunggren *et al.* 2003; Zang & Stephansson 2010). Furthermore, the assumption of a critically stressed crust is often made but is likely to overestimate the stress S_{Hmax} magnitude (Townend & Zoback 2000; Cappa & Rutqvist 2012). Thus, these data may result in a low accuracy of the model results, that is the model is not particularly correct in its prediction (Fig. 1).

To account for the stress magnitude uncertainties Ziegler & Heidbach (2020) define a probability distribution function for these data and Lecampion & Lei (2010) use Bayesian statistics. These approaches leave us with a solution space with a probability distribution of the stress state.

Ziegler & Heidbach (2023) expanded the Bayesian approach using additional stress information to further constrain and narrow down the solution space, that is to increase the precision of the model results. This additional information are upper and lower boundaries of the stress magnitudes derived from formation integrity tests (FITs), observed seismicity as well as borehole breakouts (BOs) and drilling induced tensile failures (DITFs; Bell & Gough 1979; Amadei & Stephansson 1997; Aadnoy & Bell 1998; Schmitt *et al.* 2012). In particular, BOs and DITFs have the advantage that they sample a larger rock volume when they are traced along the borehole trajectory. In the following, we call this additional data indirect stress information and stress magnitudes direct stress data. The remaining problem is, however, that the initial solution space is determined by stress magnitude data. Given the usually very low number of stress magnitude data that are available in a model volume even a single outlier can shift the solution space significantly.

This problem is visualized in Fig. 2. Assuming that some stress magnitude data are not representative, have underestimated uncertainties, or are simply erroneous, the resulting best-fitting solution (Fig. 2a) and the solution space with a probability distribution (Fig. 2b) is not accurate. The unknown real solution (green circle in Fig. 2) is potentially not even within the proposed solution space (orange ellipse in Fig. 2). Further constraining the solution space to increase the precision of the model results, as proposed by Ziegler & Heidbach (2023) and shown in Fig. 2(c) cannot solve the problem; the accuracy remains low as the unknown real solution is outside the investigated solution space.

Another obvious limitation of the approach that is that it cannot be used if no stress magnitude data is available. This is also a situation commonly found in models at reservoir scale (Ziegler *et al.* 2016; Morawietz *et al.* 2020)

Here we present a different approach to overcome these limitations. Instead of relying on stress magnitude data for the initial definition of the solution space (Figs 2a–c), we start with a solution space that contains all horizontal displacement boundary conditions that are physically reasonable (grey area of Figs 2a–c). As sketched in Fig. 2(d) we then narrow the solution space by assessing for each pair of boundary conditions within the grey area how likely they are using both data types, the direct stress data (stress magnitude) and indirect stress information (BOs, DITFs, FITs and seismicity). To both data types we apply in a formalized way a Bayesian weighting scheme that has been presented in Ziegler & Heidbach (2023). Where appropriate, we refer to them for an in-depth description.

We test and validate the new workflow using a generic 3-D model with known results (truth model) and show that anomalous stress magnitude data are correctly identified as outliers. We then apply the workflow to a case study in the Bavarian Molasse and compare the results to a published model result with estimated uncertainties that uses the procedure of Ziegler & Heidbach (2023) as sketched in Figs 2(a)–(c). The results of the truth model as well as the one from the case study show that the new approach gives similar results and can be used without constraints while at the same time provides significant and new insights into the geomechanics of a model region. A byproduct of the new approach is a significant decrease of required CPU time as we perform most of our calculations analytically.

2 METHODOLOGICAL APPROACH

With a given geometry and lithology, a single pair of horizontal displacement boundary conditions in *x*- and *y*-direction results in a

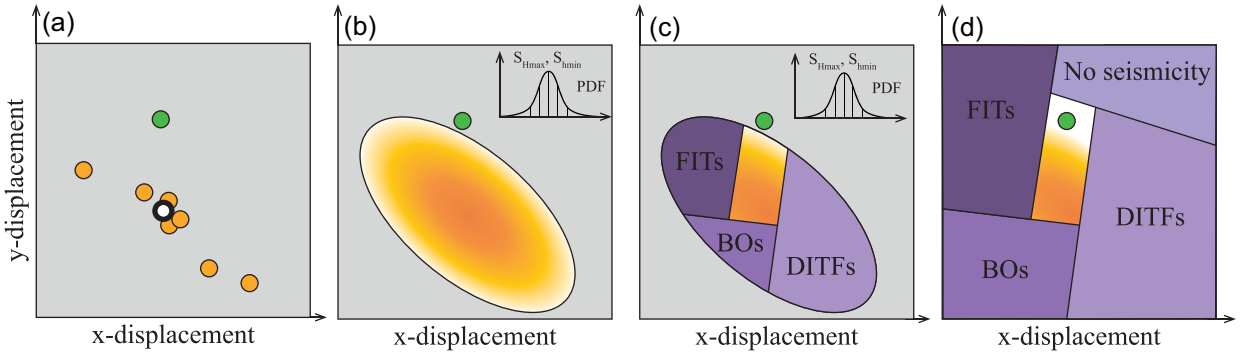

Figure 2. Conceptualization of the solution space approach. Grey square displays the solution space that contains all physically reasonable horizontal displacement boundary conditions to solve eq. (1). Green point is the unknown real solution. (a) Orange points are pairs of horizontal displacement boundary conditions that result in a perfect fit of pairs of stress magnitudes of the maximum and minimum horizontal stresses S_{Hmax} and S_{hmin}, respectively (Ziegler & Heidbach 2020; Ziegler *et al.* 2023; for technical details), white, bold circle is the best-fitting solution (Reiter & Heidbach 2014; Ziegler *et al.* 2016; Ahlers *et al.* 2022). (b) Accounting for uncertainties in each stress magnitude data record with a probability density function according to its quality and reliability the best-fitting solution space (orange ellipse) is defined (Ziegler & Heidbach 2020). (c) Borehole Breakouts (BOs), Drilling Induced Tensile Fractures (DITFs), Formation Integrity Tests (FITs) and observed seismicity can be used as additional stress information to narrow down the best-fitting solution space. (d) Alternative approach presented in this paper starting with an unlimited solution space (grey background) which is then narrowed by exclusion of impossible stress states identified by direct and indirect stress information in a Bayesian framework to estimate to most likely solution space.

unique but laterally anisotropic stress state within the model. This is herein referred to as model scenario (Fig. 3). This stress state is the response of lithology in terms of rock properties and the geometry of the lithologies to the boundary conditions. Instead of estimating the horizontal displacement boundary conditions that result a best fit with respect to the stress magnitude data, we define an initial solution space that is based on a regular grid in the domain of boundary conditions that sample all physically reasonable stress states (grey stars in Fig. 3a). This results in a large number of model scenarios. However, for computational and handling reasons, the number of model scenarios and therefore the solution space needs to be constrained.

In a first step, the solution space is constrained to all physically reasonable stress states. The term reasonable is used in the sense that a stress state is theoretically possible, but it does not have any implications whether it makes sense from a regional geomechanical or tectonic perspective. This means, that those stress states that fundamentally violate our understanding of geomechanics in general or the area of interest in particular can already be excluded. Reasons for exclusion are for example: (1) High negative stresses (i.e. tensional stresses) at depths. (2) Unreasonably high stresses in particular close to the surface. (3) In models with an observed stable S_{Hmax} orientation, a 90° rotation is not allowed, that is a switch of the S_{Hmax} and S_{hmin} orientation.

In a second step the remaining physically reasonable stress states in the solution space are evaluated how likely they are. This is done by means of indirect stress information from BOs, FITs, DITFs or seismicity (Fig. 4; Ziegler & Heidbach 2023). All physically reasonable stress states are compared to this data type and the agreement or disagreement is recorded. To identify the most likely stress state, the rates of agreement from the indirect stress information are combined in a Bayesian approach to estimate a posterior probability as a final weight following the work by Ziegler & Heidbach (2023). The probability of a model scenario P(S|C) is called the posterior probability and is estimated by

$$P(S|C) = \frac{P(C|S)\ P(S)}{P(C)} \tag{4}$$

With the likelihood P(C|S) defined as previously mentioned rate of agreement with indirect data. The probability of stress states P(S) is called the prior probability and can be either based on the tectonic stress regime as a rather broad weighting or more detailed based on available stress magnitude data, or on both. However, prior probabilities are not required if no data is available at all, that is in theory, the geomechanical model can be setup without any stress magnitude data. Even though in that case no Bayesian weighting is possible, and the approach can be applied when only indirect data are available. Eventually, the indirect stress data's quality is weighted and assigned as the Bayesian marginal probability P(C).

3 GENERIC 3-D MODEL

To test and validate the described approach we use a 3-D generic model with pre-defined synthetic stress data records with additional noise. This allows an assessment of the benefits and limits of the approach by using a model where the results are already known in the sense of truth modelling. Furthermore, we use this generic model to show that the approach can identify potential outliers of the model calibration data.

3.1. Model geometry and rock properties

The model geometry reflects a typical geo-reservoir setting on a scale of 5 × 5 × 4 km^3. It has three different lithologies, two synthetic vertical boreholes where direct and indirect stress information is defined, and we assume the occurrence of seismicity within the model volume (Fig. 5). The linear elastic properties and density for the three layers is given in Table 1.

The model is discretized with a regular hexahedral mesh that consists of 16 000 finite elements. The orientation of S_{Hmax} is assumed to be N–S, that is parallel to the *y*-axis. It is assumed that the stress state within the generic model is correctly modelled applying gravity and using the horizontal displacement boundary conditions of *X*: −5.87 m and *Y*: 6.11 m. Within the two synthetic boreholes stress magnitude data are defined. Furthermore, indirect stress information is provided by BOs, DITFs, FITs, and seismicity, but these data will be introduced later in detail when they are used to narrow the solution space.

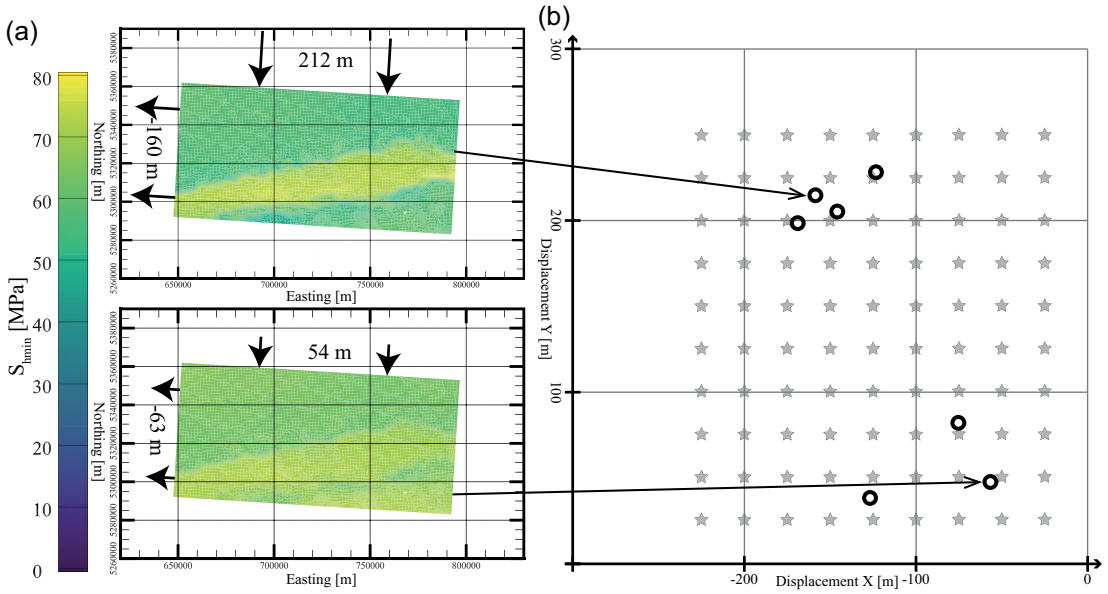

Figure 3. (a) Colour-coded S_{hmin} magnitude on a plane in 3000 m depth in two different model scenarios from the 3-D geomechanical-numerical model of the Bavarian Molasse Basin (Ziegler & Heidbach 2023). Both model scenarios are supported by different stress magnitude data. Each model scenario can be unambiguously identified by the applied horizontal boundary displacement in *x*- and *y*-direction. (b) Boundary conditions are used to situate different model scenario in a solution space in terms of the applied boundary conditions (circles). Contradictions in stress magnitude data used for calibration result in quite different boundary conditions and resulting stress states. Due to the expected large uncertainties in stress magnitude data, it is advisable to not only evaluate the boundary conditions that result from fitting stress magnitude data. It is beneficial to use regularly spaced boundary conditions (grey stars) for model evaluation in order not to miss the actual stress state.

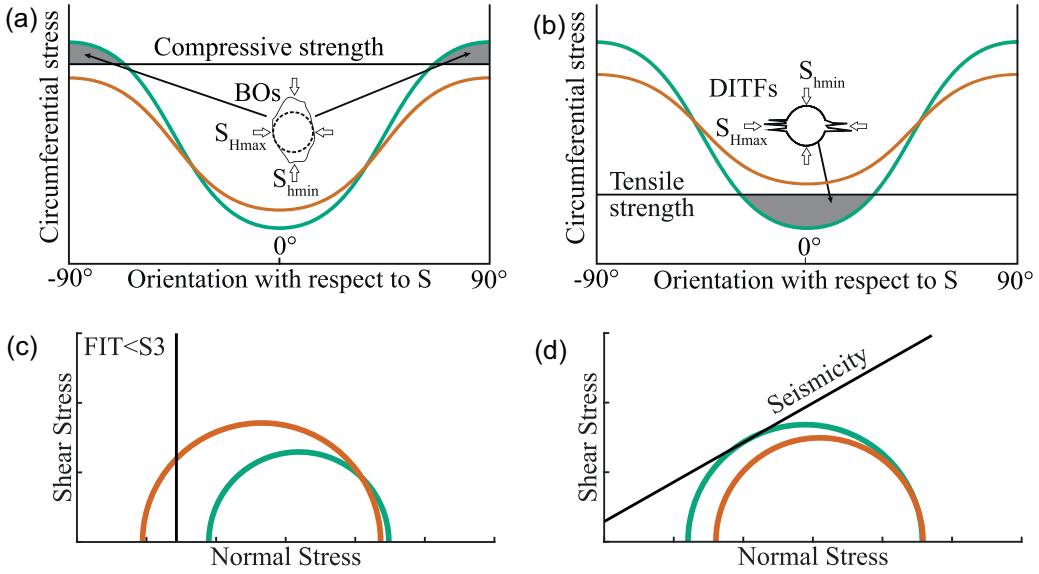

Figure 4. Two modelled stress states (red and green graphs) in comparison with four different types of indirect stress information (Ziegler & Heidbach 2023). (a) Borehole Breakouts (BOs) indicate that the maximum circumferential stress around the borehole wall exceeds the compressive strength of the rock. (b) Drilling Induced Tensile Fractures (DITFs) indicate that the minimum circumferential stress around the borehole wall is smaller than the tensile strength of the rock. (c) Formation Integrity Tests (FITs) provide a lower limit for the smallest stress component. (d) Seismicity indicates that the failure envelope of a given criterion has been reached.

A model scenario is defined as the stress state that results from the solution of eq. (1) for a given set of horizontal displacement boundary conditions. The full range of model scenarios to be assessed is defined by the boundary conditions from the solution space. To test the full range of the solution space many model scenarios would have to be tested for their agreement or disagreement with the additional stress information. To be able to estimate the stress state for distinct locations with data for the large number of model scenarios in a reasonable time frame, we chose a limited number of distinct locations and use the Python tool FAST Estimation and FAST Calibration both described and documented in detail by Ziegler (2023a) and Ziegler *et al.* (2023). Both tools use the assumption of linear elastic behaviour of the stress model to set up a linear equation system based on three model scenarios with arbitrary horizontal displacement boundary conditions. This linear equation system allows to derive analytically the 3-D stress state for all reasonable

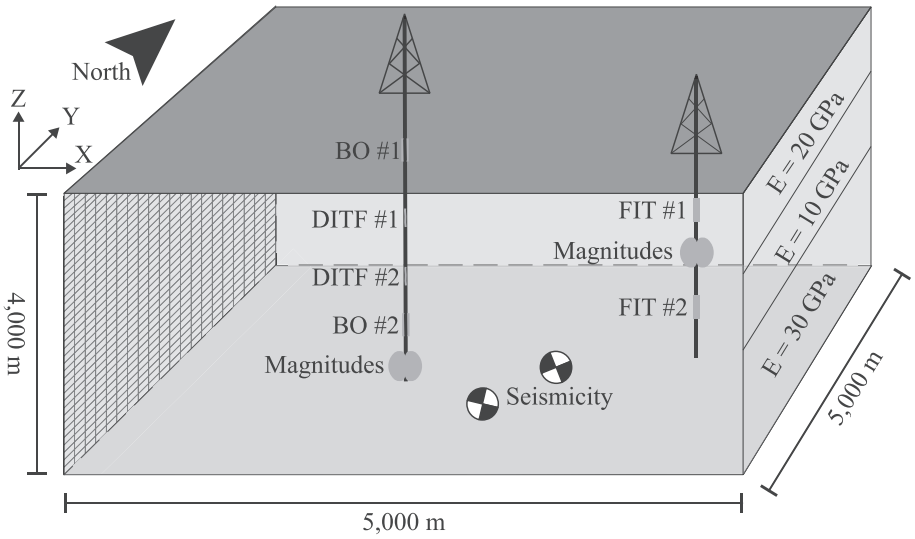

Figure 5. Geometry and data availability of the 3-D generic model. Discretization is indicated on the western boundary of the model, lithology mapped to elastic properties on the eastern boundary. Synthetic stress information data are indicated throughout the model volume and their numbers are compiled in Tables 2 and 3.

Table 1. Linear elastic rock properties and density of the three lithologies.

Lithology	Young modulus [GPa]	Poisson's ratio	Density [kg m^{-3}]
1	20	0.250	2350
2	10	0.290	2500
3	30	0.225	2600

combinations of boundary conditions at a limited number of distinct locations. This enables us to significantly speed up the process of modelling by only solving the stress state for the locations where data is available for comparison.

3.2. Initial solution space definition

Initially, we consider all stress states that are theoretically possible but without assessing if they make sense from a geomechanical or tectonic perspective. For the generic model an evenly spaced grid of horizontal displacement boundary conditions is created with a grid size of 1 m (Fig. 6). Then, the stress states for each model scenario in this grid are computed at representative locations in different depths throughout the model using the Python tool FAST Estimation (Ziegler 2023a).

We show in Fig. 6 along six vertical profiles the model results determined from different boundary conditions throughout the solution space. Three of them can be considered to represent reasonable stress states (Figs 6b, e and f) and three show unreasonable stress states (Figs 6c, d and g). The latter may fundamentally violate our understanding of the stress state in the brittle upper crust and can be excluded to constrain the solution space. The following rules are observed when selecting the reasonable boundary conditions.

Model scenarios where at more than 30 per cent of the representative locations stress estimates are negative are discarded (Fig. 6d). The generous cut-off at 30 per cent allow for some negative magnitudes close to the topography that may be due to surface effects. In addition, exceptionally large stress magnitudes ($>$100 MPa) in shallow regions ($<$100 m TVD) are neither considered realistic and thus respective model scenarios are also discarded (Fig. 6c). These two constraints cannot be defined precisely and largely depend on the local geology. The cut-off needs to be defined individually dependent on factors such as roughness of the topography. In a model area with significant and rapid changes in elevation, topography effects can lead to large stresses close to the surface or even tensile stresses. In a model with a flat topography this is not expected.

An inherent constraint for the initial boundary conditions are model scenarios where the S_{Hmax} orientation is not as expected, for example it is rotated compared to observations from the field (Fig. 6g). This constraint may only be applied in areas with an unambiguous predominant orientation of S_{Hmax}. In synthesis, these limiting factors constrain the boundary conditions that result in reasonable stress states (coloured dots in Fig. 6a) and discards those that are not reasonable (grey dots in Fig. 6a). Result is the solution space that is assessed in the following to find likely stress states by using indirect stress information and direct stress data. The solution spaces grid spacing of initially 1 m is increased to a spacing of 0.5 m albeit only in the area of reasonable stress states shown in Fig. 6(a).

3.3. Introduction of indirect stress information

In the previous step, the solution space was narrowed to a reasonable one to start with. Now, the task is to further narrow this solution space using indirect stress information to find likely stress states. For the generic modelling approach, a number of generic indirect stress information that agrees with the anticipated true stress state is used for this constraining (Table 2). Each horizontal displacement boundary condition defines a unique stress state. Thus, for each of these model scenarios, the resulting stress states have to be tested for their agreement with indirect stress information at the location where it is available. In order to limit the computation time to a reasonable time frame, an actual solving of all models that are defined by the boundary conditions is not possible. Instead, the above mentioned tool FAST Estimation (Ziegler 2023a) is used to compute the stress state for each reasonable boundary condition but in contrast to Ziegler & Heidbach (2023) only at the distinct locations and depths where indirect stress data is available.

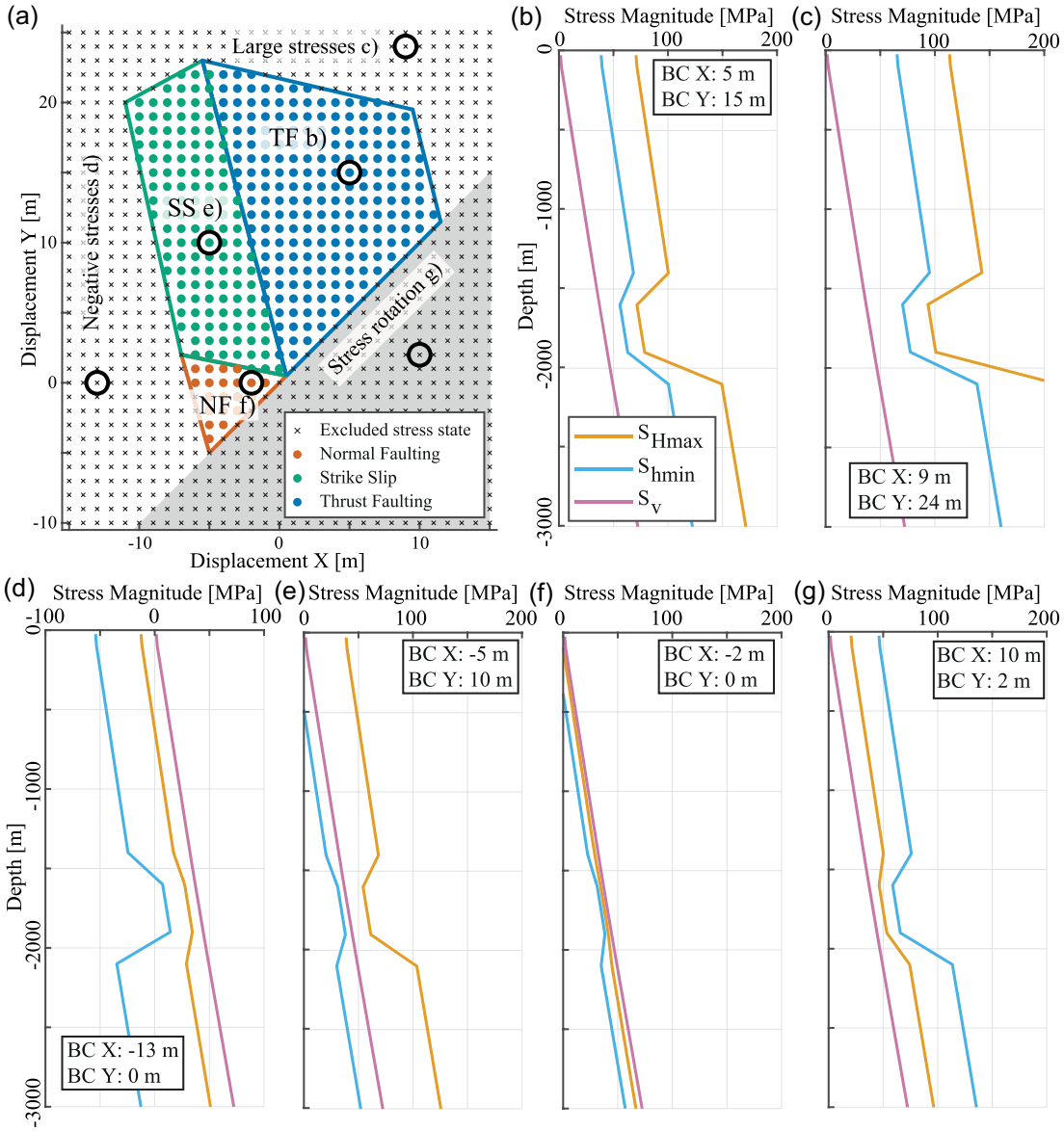

Figure 6. Evaluation of possible stress states and implementation of hard constraints displayed in the solution space domain of the horizontal boundary conditions with the three tectonic stress regimes and boundary conditions that result in such a stress regime are colour coded for normal faulting (NF, red), strike slip (SS, green) and thrust faulting (TF, blue) (a). Stress-depth plots resulting from the boundary conditions indicated by the circles in (a) with S_{Hmax} (orange), S_{hmin} (light blue) and S_{v} (pink) (b–g). Tectonic stress regimes normal faulting ($S_v > S_{\mathrm{Hmax}} > S_{\mathrm{hmin}}$, f), strike slip ($S_{\mathrm{Hmax}} > S_v > S_{\mathrm{hmin}}$, e) and thrust faulting ($S_{\mathrm{Hmax}} > S_{\mathrm{hmin}} > S_v$, b) are indicated. Furthermore, constraints are implemented that rule out unrealistic stress states such as largely negative stresses (d), extremely large stresses (c), or a rotation of the S_{Hmax} orientation, herein indicated by the stress in the S_{hmin} orientation that has a magnitude that is larger than the stress component in the S_{Hmax} orientation(g and grey area in a).

Table 2. Synthetic indirect stress information used to assess the reliability of a modelled model scenario in the generic model. Different types, the locations, relevant values and weight of the individual records are indicated.

Type	X [m]	Y [m]	Z [m]	Values	Weight
Bos	−2000	1500	−1750	$C_{\mathrm{s}} = 70 \pm 5$ MPa	0.4
	−2000	1500	−3500	$C_{\mathrm{s}} = 200 \pm 20$ MPa	0.9
DITFs	−2000	1500	−1900	$T_{\mathrm{s}} = 13 \pm 2$ MPa	0.9
	−2000	1500	−2800	$T_{\mathrm{s}} = 4 \pm 2$ MPa	0.4
FITs	−2000	−2000	−1750	25 MPa	1
	−2000	−2000	−3500	50 MPa	0.7
Seismicity	0	0	−2200	$C = 0$ MPa, $\mu = 0.6$	1

At each location with available indirect stress information the stress state that results from each boundary condition is now available. These locations are usually not identical with the previously used representative locations throughout the model since the available data is not necessarily distributed in a way that it is representative for the entire model volume. The indirect stress information is compared with these modelled stress states following the approach described in detail by Ziegler & Heidbach (2023). The agreement or disagreement with a stress state defined by a certain boundary condition is recorded. It can be displayed for each individual data record, for example each individual borehole wall section that contains a breakout, but also for each type of indirect stress information, for example for all breakouts in all boreholes.

Which boundary conditions are rejected or supported by indirect stress information is highly dependent on the type of stress indicator. While some stress indicator may primarily affect the boundary conditions in only one direction, they also always affect the boundary condition in the other direction. Thus, the boundary conditions should not be mathematically equated with the stress magnitudes. Details on the relationship between boundary conditions and the stress components can be found in, for example Reiter & Heidbach (2014), Ziegler & Heidbach (2020) or Ziegler *et al.* (2023). Still, it can be observed that FITs reject boundary conditions with small displacements in orientation of S_{hmin} (Fig. 7a) since these boundary conditions are predominately responsible for small S_{hmin} magnitudes which are constrained by FITs (Fig. 3c). DITFs reject those model scenarios with large displacement in orientation of S_{hmin} that result in large magnitudes of S_{hmin} (Fig. 7a). Following the Kirsch equation (Kirsch 1898) the minimum circumferential stress around a borehole wall is

$$\sigma_{\varphi\varphi}^{\min} = 3\,S_{\mathrm{hmin}} - S_{\mathrm{Hmax}} - P_w - P_p \tag{5}$$

with the mud pressure P_{w} and the formation pore pressure P_{p}. $\sigma_{\varphi\varphi}^{\min}$ needs to exceed the tensile strength of the rock in order for DITFs to occur. Eq. (5) indicates that an increase in S_{hmin} magnitude results in an increase in $\sigma_{\varphi\varphi}^{\min}$. Thus, for S_{hmin} magnitudes that are close to the S_{Hmax} magnitude DITFs become less probable. Thus, FITs and DITFs are valuable counterparts that narrow down the range of reasonable boundary conditions roughly applied in the orientation of S_{hmin}.

BOs prefer large displacements in the orientation of S_{Hmax} and reject small ones (Fig. 7a). This is analogously to the DITFs. BOs form if the maximum circumferential stress around a borehole wall $\sigma_{\varphi\varphi}^{\max}$ exceeds the compressive strength of the rock. From

$$\sigma_{\varphi\varphi}^{\max} = 3\,S_{\mathrm{Hmax}} - S_{\mathrm{hmin}} - P_w - P_p \tag{6}$$

it becomes apparent that an increase in S_{Hmax} magnitude leads to an increase in $\sigma_{\varphi\varphi}^{\max}$ and thus BOs become more likely.

Observed seismicity indicates that the stress state exceeded a failure criterion on a new or pre-existing fault. This failure can be simplified and described with the slip tendency

$$\mathrm{ST} = \frac{\tau_{\max} - C}{\sigma_n}\mu^{-1}, \tag{7}$$

where $\tau_{\max}$ and σ_{n} are the maximum shear stress and normal stress of the fault, respectively, μ is the static friction coefficient, and C the cohesion (Morris *et al*. 1996, Ziegler *et al.* 2016a, b). Failure occurs if ST $\geq$ 1. Otherwise, the rock remains stable. If seismicity is observed, the modelled stress state can be used to estimate ST. If ST $\geq$ 1, it is assumed that model and observation are in agreement. This constraint rejects the lower right-hand corner of the solution space that indicates high displacements in S_{hmin} and low displacements in S_{Hmax} orientation (Fig. 7a). This part of the solution space is associated with small differential stress which prevents seismicity.

Eventually, the weights from all indirect stress information are combined for a final weight of the stress states according to the indirect stress information (Fig. 7b). In association, the different types of indirect stress information have the potential to significantly narrow down the likely stress states. Depending on the types, uncertainties, and characteristics of indirect stress information this can be a more or less broad range of stress states. Details on the assessment of the agreement/disagreement and on how uncertainties in the indirect data are implemented are explained in Ziegler & Heidbach (2023). If no suitable stress magnitude data or information on the tectonic stress regime, that can serve as direct data are available, this is the final result.

3.4. Bayesian weighting

The range of likely stress states is, at this point, not based on any stress magnitude data. If such data is available as well it can be used to further constrain the likely stress states (Figs 2d and 8). On a lower information level, even knowledge of the predominant tectonic stress regime can be useful and included as Bayesian prior probability (Figs 6 and 8) to a Bayesian weighting scheme initially presented by Ziegler & Heidbach (2023). The posterior probability P(S|C) of a model scenario S that is constrained by indirect stress information C is estimated by

$$P(S|C) = \frac{P(C|S)\;P(S)}{P(C)} \tag{8}$$

with P(C|S) the likelihood of the indirect stress information as additional constraint in the model scenario, that is does the indirect stress information agree with a scenario's modelled stress state. For an FIT this can be exemplified by a simple 0 for disagreement or 1 for agreement (Fig. 9). Other indirect information that require additional assumptions may have a more distinguished assignment procedure of P(C|S) such as for BOs (Fig. 9). P(C) is the marginal probability of the according indirect data. It is a measure of the correctness and predictive quality of the data record under the given circumstances. P(C) is assigned individually to each indirect stress information evaluating the data itself but also the circumstances of measurement, used tools and availability and quality of metadata to assign an objective quality of the data record. Information on the probability of a model scenarios stress state is introduced as prior probability P(S). It can be based on stress magnitude data records (Ziegler & Heidbach 2023) which then employs a quality ranking to assign weights to the individual data records (Morawietz *et al.* 2020). Furthermore, information such as the tectonic stress regime can be used. The assignment of such weights is based on seismological data mainly in the latter case.

The resulting posterior probability P(S|C) is estimated for each individual stress state and provides an indication of the individual predictive quality of a stress state. Eventually, the model scenarios with the most probable boundary conditions can be solved in a numerical solver in order to obtain the stress tensor throughout the entire model volume.

To illustrate the approach with using direct data, for the generic model stress magnitude data records with an assigned probability weight are used (Table 3). These data are used to assign an initial weight to each model scenario (Fig. 8a) based on how well it represents the stress magnitude data at the according location. Furthermore, assumptions on the tectonic stress regime are made (Fig. 8b).

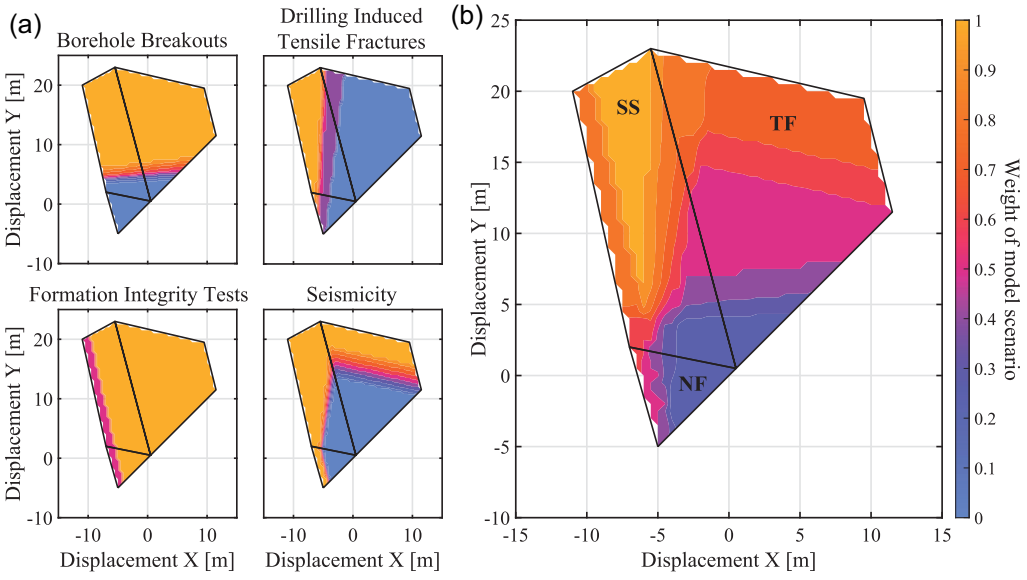

Figure 7. Agreement of the different model scenarios with the individual types of indirect stress information (a) and all indirect stress information combined (b). Each colour-coded dot represents one of the 1517 individual model scenarios based on the respective horizontal displacement boundary conditions indicated on the *x*- and *y*-axis. The colour shows the weight of the model scenarios from 0 (very unlikely, reject) to 1 (highly likely, full agreement) and is based on the additionally specified constraints—thus only valid for this model configuration. Bold black lines indicate the likely solution space and the borders between the dominant stress regime (Fig. 6). The according stress regimes are indicated by the abbreviations in (b).

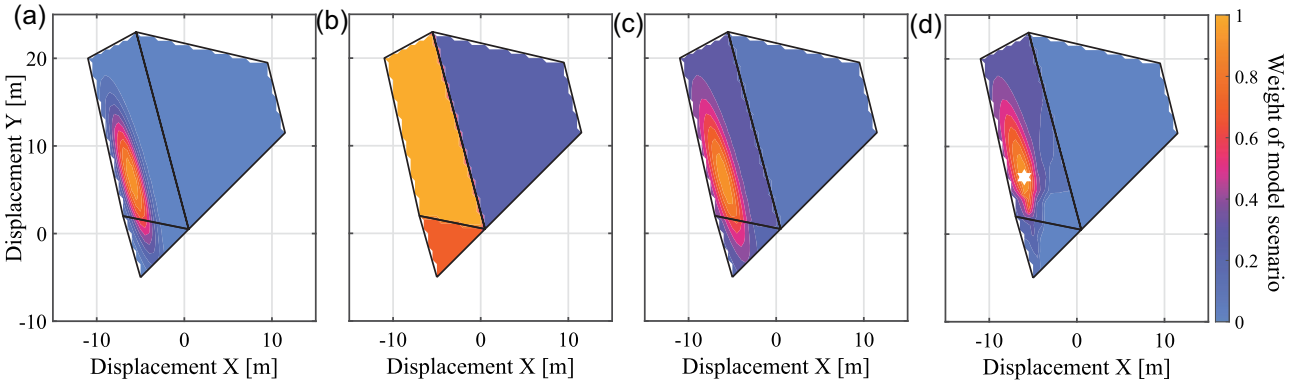

Figure 8. Bayesian prior probabilities. Initial weighting of the model scenario solely based on stress magnitude data (a) or the assumed tectonic stress regime (b). A combination of stress regime and magnitude data is used as prior probability in a Bayesian approach (c). The posterior probability (final weight) that also considers the indirect stress information and its quality is shown in (d). For a detailed explanation of the plots refer to the caption of Fig. 7.

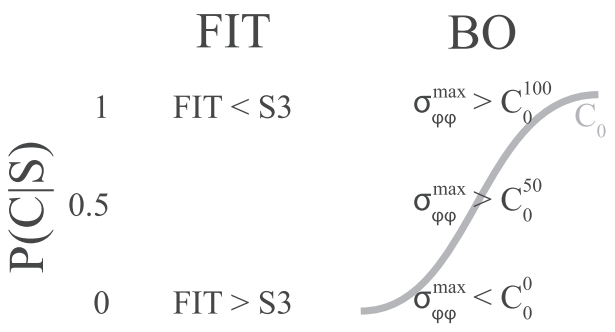

Figure 9. Assignment of P(C|S) exemplified for FITs and BOs. While FITs are a binary decision between 0 (disagreement) and 1 (agreement), for BOs a cumulative density function (CDF) of the rocks compressive strength can be assigned. P(C|S) depends on the maximum circumferential stresses position in the CDF.

In the generic truth model, a strike slip regime is assumed to be most likely with a weight of 1 and a normal faulting stress regime is still possible with a weight of 0.75. A thrust faulting stress regime can be almost ruled out with a weight of 0.25. These two parts of direct data are combined. In this example, the stress magnitudes have twice the influence compared to the stress regime (Fig. 8c). The combined direct data is introduced to the Bayesian scheme as P(S), the indirect stress information as P(C|S) (Fig. 7b), and the probabilities of the indirect stress information as P(C) (Table 2) in order to estimate the final Bayesian weight P(S|C) (Fig. 8d).

The results show a good agreement with the true boundary conditions of *X*: −5.87 m and *Y*: 6.11 (Fig. 8d). The stress regime is clearly identified as strike slip by the indirect data (Fig. 7b) while a normal faulting stress regime cannot be ruled out by the direct data (Fig. 8c). This shows the applicability of the approach and its ability to significantly constrain the stress state. At the same time the large influence of direct data on the final result is displayed.

Table 3. Stress magnitude data records used as prior probabilities in the Bayesian approach. Coordinates, magnitude, and a weight that is based on the degree-of-belief in the data record is indicated. Last column shows stress magnitude data with an added noise in order to test the sensitivity of the approach.

Stress comp.	X [m]	Y [m]	Z [m]	Magnitude [MPa]	Weight	Noisy magnitude [MPa]
S_{Hmax}	1500	1500	−1300	49	0.7	90
	−2000	−2000	−4000	123	0.4	140
S_{hmin}	1500	1500	−1300	10	0.8	50
	−2000	−2000	−4000	64	0.6	90

4 DISCUSSION

The presented approach removes the focus from the stress magnitude data which previously have been identified as one of the most, if not even the most important input data for geomechanical-numerical models (Wileveau *et al.* 2007; Lecampion & Lei 2010; Fischer & Henk 2013; Reiter & Heidbach 2014; Hergert *et al.* 2015; Morawietz *et al.* 2020; Ziegler & Heidbach 2020). Instead, this approach uses a wide range of indirect stress information beyond stress magnitude data to model the *in situ* stress state with quantified uncertainties.

On the one hand, this is beneficial in that more data can be used for model calibration and the uncertainties and possible outliers in magnitude data are more easily identified and accounted for. The full range of possible stress states can be easily assessed, and even different principles can be accommodated, such as a stress state based on S_{Hmax} and S_{hmin} stress magnitude data or a critically stressed crust based on S_{hmin} magnitude data only. That said, the accuracy of the model result increases due to several independent types of input data that can identify systematic offsets or errors in stress magnitude data or other indirect stress information. At the same time, precision may even decrease due to the larger amount of considered and likely stress states.

On the other hand, the now used indirect stress information are subject to (sometimes significant) uncertainties, too. This calls for an investigation of the sensitivity of the approach to assumptions made and uncertainties. In particular, BOs and DITFs are affected due to the necessary assumptions on the rock strength (Bell & Gough 1979; Ziegler & Heidbach 2023). Observed seismicity is also significantly affected by uncertainties due to necessary assumptions on fault properties in the model and the inherent challenges in observation of seismicity (Ziegler & Heidbach 2023). FITs, in contrast, are rather robust due to the simple reading of a pressure.

4.1. Sensitivity of the approach

BOs can be easily identified and picked in borehole image and caliper logs. Contrary to usage as stress indicators for the S_{Hmax} orientation (Barton *et al.* 1988; Vernik & Zoback 1992), their use as indirect stress information does not require a highly precise estimation of width of the angle of the BO, a preferably vertical well, or other assumptions. The simple knowledge of whether a BO occurred in a certain lithology or not is sufficient here. Yet, uncertainties are associated with this type of indirect stress information as well since at least assumptions on the rock strength and the failure criterion have to be made (Rahimi & Nygaard 2018). Furthermore, influence of factors such as borehole diameter are known (Meier *et al.* 2013) as well as the time-dependency of BOs have to be considered (Rajabi *et al.* 2017). Unfortunately, seldom are laboratory tests of exactly the same lithology (or even from the same location) where BOs are observed available. This drives the uncertainties in the compressional rock strength. In order to demonstrate the influence of these uncertainties on the weighting results, different assumptions on the rock strength were made and the results are shown in Fig. 10. This shows a high sensitivity and reminds to carefully chose the assumed compressive strength. This is analogous for the tensile strength when using DITFs.

When observed seismicity is used as indirect stress information in particular the depth error of the hypocentre has to be considered as it affects the exact lithology that has to be considered to obtain the stresses relevant to assess whether failure occurs or not. Furthermore, the assumed fault orientation is an important factor as it determines the resolved shear and normal stresses on the fault from the modelled 3-D stress state which control the reactivation (Morris *et al*. 1996; Ziegler *et al.* 2016a, b). An additional leverage on the estimation whether a fault fails or not is the assumed fault friction and cohesion, that is whether a pre-existing fault or a new fracture is regarded (Morris *et al*. 1996; Ziegler *et al.* 2016a, b). The large influence of different standard fault properties on the weighting is displayed in Fig. 11. It indicates the necessity to mindful assignment of properties and to leave room for uncertainties in these properties.

4.2. Identification of erroneous stress magnitude data

The direct data introduced to the approach are as well a possible source for uncertainties or errors. Uncertainties are already regarded in the assignment of prior probabilities in the Bayesian approach based on stress magnitude data. However, the underlying assumption was that the data are generally correct and only some outliers or single errors have to be regarded.

However, stress magnitude data can be significantly and systematically wrong either because of measurement errors or the measurement at a meter scale is not representative for a larger rock volume. The effect of such data on the weighting pattern and whether the approach is able to identify them is investigated here. The weighting pattern created by erroneous stress magnitude data is shown in Fig. 12(a). Even with a correctly assumed tectonic stress regime, they result in a very different final weighting result (Fig. 12b compared to Fig. 8d). It is easily noted that the maximum weight in Fig. 12(b) falls short of 1 which signifies that no complete agreement between direct and indirect stress information is observed. Furthermore, a visual comparison between Figs 12(b) and 7(b) shows a significant discrepancy between the patterns produced by indirect stress information and direct stress data. In case of correct stress magnitude information but a wrong preference for a thrust faulting stress regime (TF: 1, SS: 0.75, NF: 0.5) the results are not as strikingly different (Fig. 12c). The most likely model scenarios are still positively identified. The main errors occur for areas that are

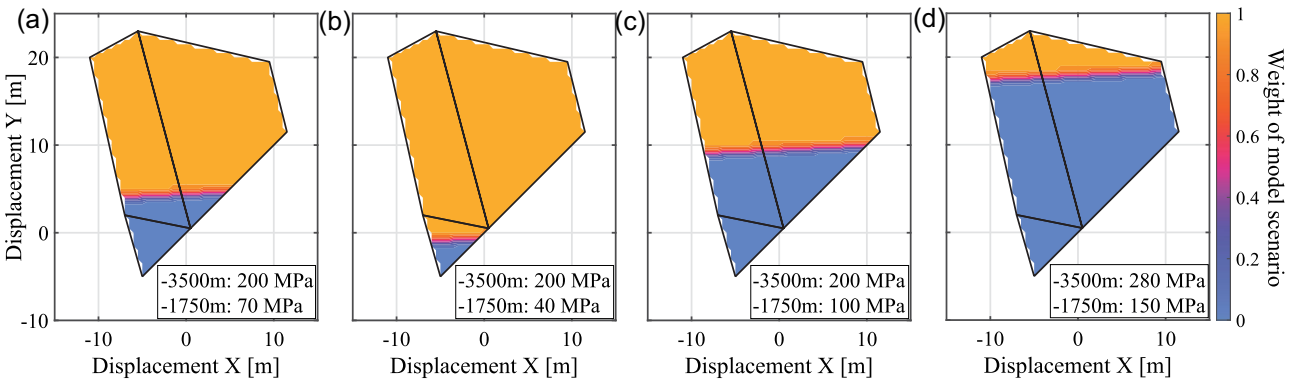

Figure 10. Sensitivity of model scenario weights based on BOs and different compressive strength in two model lithologies. The initially assumed strength (a) and deviations from this (b–d). Only one lithology is affected by a smaller strength (b) and greater strength (c). Both lithologies are affected by a larger strength in (d).

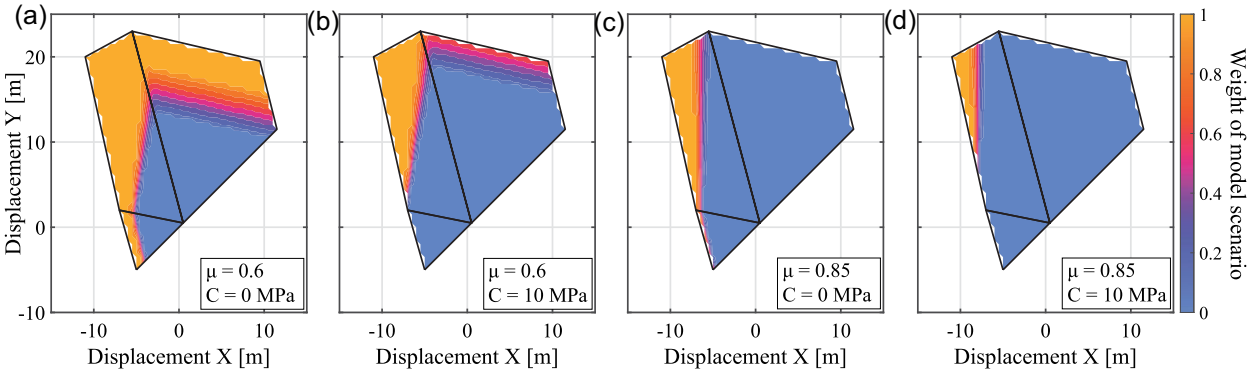

Figure 11. Sensitivity of weights based on observed seismicity on the assumed cohesion and friction angle. The initially assumed values for a pre-existing cohesion-less fault (a) are compared to an added cohesion (b), an increased friction angle (c) and both (d).

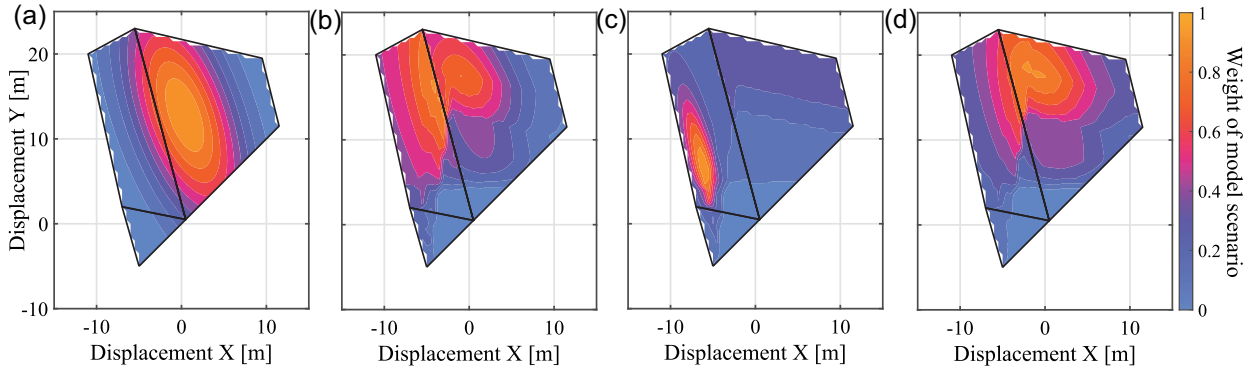

Figure 12. Dependency of the Bayesian weighting approach on the prior probabilities. (a) Significantly differently assumed stress magnitude data (Table 3) result in an initial weight in stark contrast to Fig. 8(a). (b) Bayesian weights based on correct indirect stress information (marginal probabilities) and direct data that are a combination of correctly chosen weights for the stress regime but the wrong stress magnitudes. (c) Bayesian weights based on correct indirect stress information and direct data that are a combination of wrongfully chosen weights for the stress regime but the correct stress magnitudes. (d) Bayesian weights based on correct indirect stress information but wrong direct data (magnitudes and regime).

anyway less likely. If all direct data is wrong, the patterns are even more different which should raise suspicion (Fig. 12d).

Even though a comparison with the correct solution cannot be made in case of an application in a real-world setting, suspicious weighting patterns can be observed. If the approach is conducted with care, the mismatch between the patterns resulting from direct data and indirect stress information will be noted and according actions can be taken. This indicates that the presented approach is able to identify stress magnitude data that are not suitable for the model calibration. It highlights that the approach needs to be conducted with care and expertize in order to correctly identify suspicious patterns, such as a general mismatch between the preferred boundary conditions according to the stress magnitude data records versus the indirect data. Any such mismatch should be carefully investigated in order to draw the according conclusions.

The interpretation of mismatches in patterns have to consider the uncertainties in the origin of the mismatch. In the worst case it is neither known whether the mismatch stems from local variations or

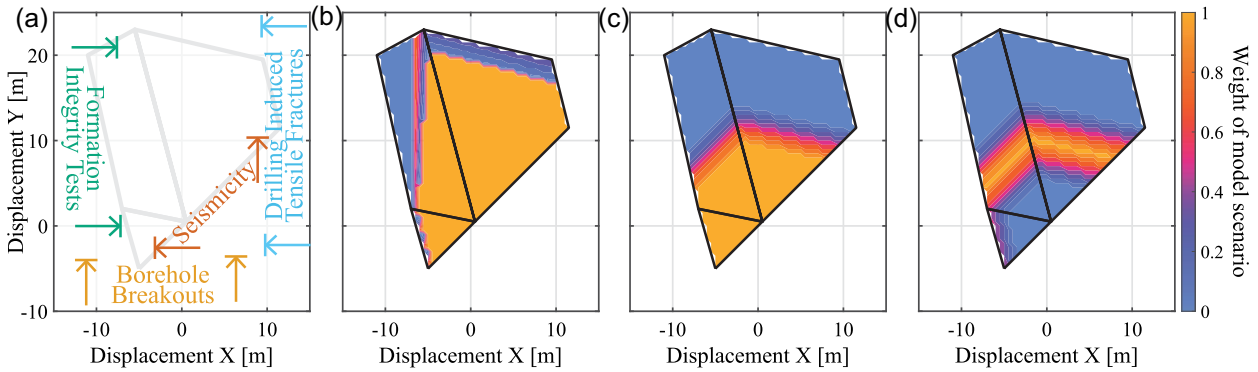

Figure 13. Need for and possible applications of additional indirect stress information. (a) The currently used indirect stress information and their constraints and areas that are excluded by them in the domain of the boundary conditions (see Fig. 7). (b) Using seismological quiescence as additional indirect stress information adds a constraint to the left and to the top. (c) Assumption on an upper limit for the differential stress provides another constraint from the top. (d) Predicted differential stress would provide an even more detailed constraint.

whether they are errors nor if the errors are in the stress magnitude data or in the indirect stress information. Expertize in the local tectonics and lithology are thus required.

4.3. Seismic events and further indirect stress information

Different indirect stress information narrows down the solution space in different ways (Fig. 13a). However, an 'upper' bound is missing to limit large positive y displacements. In other words, the so far introduced indirect stress information cannot constrain high S_{Hmax} magnitudes. To do so the observation of seismological quiescence is proposed as indirect stress information (Ziegler & Heidbach 2023). Significant care has to be taken when this is used. It must be ensured that the seismological network is dense enough and the noise level low enough in order to have a very small magnitude of completeness. Otherwise, events could be missed which would void all assumptions introduced in the constraint. Not considering these significant challenges, the introduction of such indirect stress information would indeed add an upper constraint to the weighting approach (Fig. 13b). This could be a very helpful tool, in particular in areas that are proven to be seismologically quiet. However, great care needs to be taken when working with this particular type of indirect stress information due to afore-mentioned challenges.

The differential stress S1–S3 as a possibility to characterize the stress state has been proposed previously (Ziegler *et al.* 2017). Information on the differential stress state can be obtained from observations around regional lithologic structures (Homberg *et al.* 1997; Reiter 2021) or for geo-reservoirs from seismological observations on the rotation of the stress tensor due to fluid injections (Martínez-Garzón *et al.* 2013, 2014). In association with assumptions on the reservoir permeability and known injection rates, a maximum differential stress that allows the observed rotation can be derived (Ziegler *et al.* 2017). Then it can be used as an additional indirect stress information that provides an upper constraint for the stress state, which also fills the mentioned gap (Fig. 13c).

Moreover, the derived differential stress—if certain enough—can theoretically additionally act as a lower and upper boundary. The derivation of the differential stress according to Ziegler *et al.* (2017) results in a single differential stress for each observed stress tensor rotation in conjunction with an assumption of permeability. Such an approach would significantly narrow down the likely stress states and enable an unprecedented significance in the modelled stress state, at least for the S_{Hmax} magnitude (Fig. 13d). However, the involved assumptions and requirements in terms of instrumentation to capture small magnitude seismic events are extraordinarily high and uncertainties involved in the process of derivation are likely high and maybe only partly known. Therefore, this remains a rather theoretical option.

Future studies should be directed towards the benefit of inclusion of additional and novel indirect data and their impact on the model results. In addition to the previously mentioned types of indirect stress information, for example indirect stress information could be based on pore pressure and particular overpressure data (Shatyrbayeva *et al.* 2023), results of time-dependent models of the geological evolution (Mahmoodpour *et al.* 2023), or even high-precision fault movement observations (Baroň *et al.* 2024).

4.4. Benefits and limits of the approach

The general approach to geomechanical modelling significantly changes with the presented method. Instead of trying to single out one or a few model scenarios that accommodate available stress data in a best-fitting sense, a maximally broad range of stress states is evaluated for their probability. This is only possible due to the increase in speed that is achieved using the Python tools FAST Estimation and FAST Calibration (Ziegler & Heidbach 2021a; Ziegler 2023a). These tools allow to assess the probability of a stress state at individual locations defined by horizontal displacement boundary conditions. Thus, a numerical solver is not needed at this stage and valuable computation time is saved by not having to solve a number of unrealistic model scenarios that will be discarded more or less right away. Instead, only the stress state at distinct locations is estimated for assessment. In the end, model scenarios that are considered likely can be solved after the weighting to obtain a continuous stress state throughout the model.

Furthermore, the presented approach adds significant value to the results of a model. First, this is due to a broader data basis that identifies likely stress states and rejects unlikely ones (Ziegler & Heidbach 2023). The statistical impact of outliers or stress measurement errors is therefore reduced. Second, having rather a range of stress states instead of a single one enables experts to interpret the stress state in terms of the local lithology and tectonics. Even though the proposed approach does not pinpoint a single model scenario, the provided range of reasonable model scenarios is significantly reduced to a range of likely stress states with a quantified probability. Concurrently, the interpretative value is increased by the ability

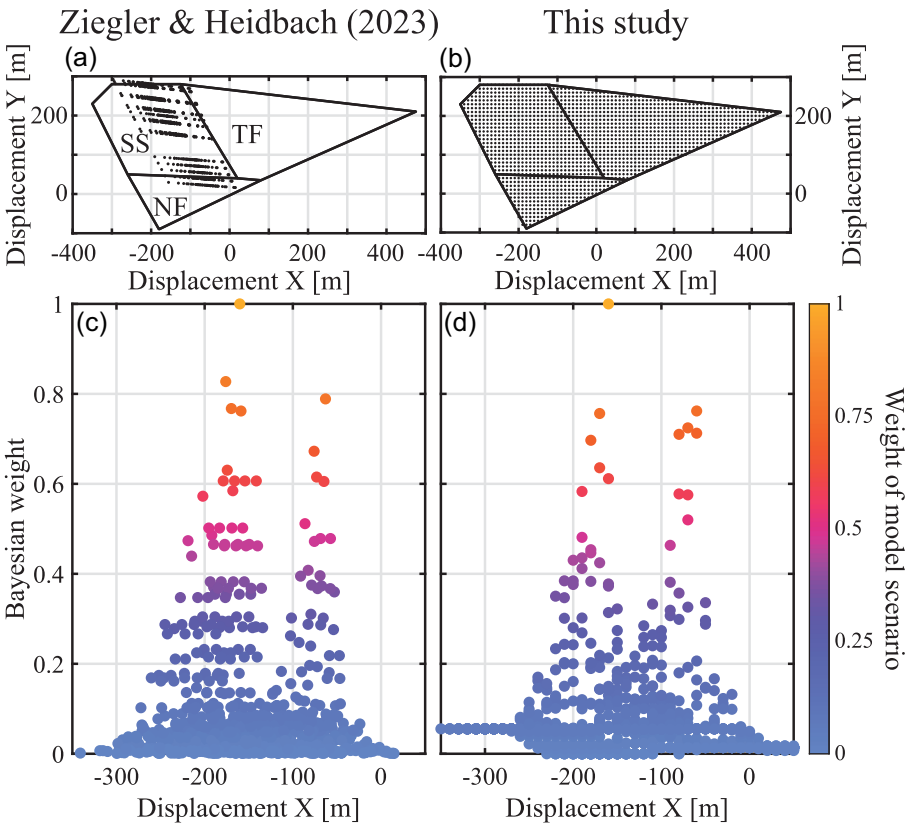

Figure 14. Comparison of the previous approach by Ziegler & Heidbach (2023) (left-hand panel) and the herein presented approach (right-hand panel). Top panel: points denote the evaluated model scenarios based on pairs of horizontal boundary conditions. The according tectonic stress regimes normal faulting (NF), strike slip (SS) and thrust faulting (TF) that result from boundary conditions are indicated Bottom panel: results are indicated by colour-coded weights from the previous approach (Ziegler & Heidbach 2023) where all evaluated stress states are based on stress magnitude data (left-hand panel) compared to the presented approach with stress states based on boundary conditions on a regular grid (right-hand panel). The horizontal displacement boundary conditions in *x*- direction on the *x*-axis and the final Bayesian weight on the *y*-axis.

to a meaningful and educated interpretation of the modelled stress state in particular due to the fact that the weighting is data-based and shows a range of possibilities.

If the approach fails to identify a single most likely horizontal displacement boundary condition, at least a range of likely boundary conditions can either be used to question if the direct stress data or indirect stress information is reasonable or to re-consider if the model has a sufficient resolution. A detailed investigation of the input data and model may resolve the issue and add significant value to the model. Possible symptoms and associated sources are:

(i) If the agreement of indirect stress information is laterally or vertically clustered some regions or lithologies may not be represented adequately in the underlying geological model.

(ii) The approach relies on an assumed linear elastic rheology which may not be adequate. Furthermore, a reliable lithological model is required and the corresponding rock properties are required.

(iii) A systematic disagreement between indirect stress information and stress magnitude data may indicate errors during the measurement and estimation of stress magnitude data. It needs to be ensured that the stress magnitude data are actually representative for an undisturbed *in situ* stress state in a larger rock volume.

(iv) If the expected stress regime disagrees with the modelled one, a possible reason may be that the expectations were mainly due to data from only one lithology that may be anomalous. Alternatively, information on the stress regime is only from deep seismicity which may not be representative for a shallow model.

In summary, failures are not a setback but rather helpful in identification of the models limits and indicate room for improvement.

The heavy usage of indirect stress information in combination with a very broad range of modelled stress states that can be assessed offers new possibilities for geomechanical modelling. Even though it is still desirable to obtain stress magnitude data, a data-based modelling is now theoretically also possible without stress magnitude data. The resulting range of likely stress states will be higher compared to a model with available stress magnitude data. Nonetheless, the approach may be helpful for an initial assessment of the stress state in regions with no stress magnitude data. Future research should aim to test the limits of such an approach without stress magnitude data.

4.5. Case study

To test the approach in a real setting we use in the following the 3-D geomechanical-numerical model of the Bavarian Molasse Basin

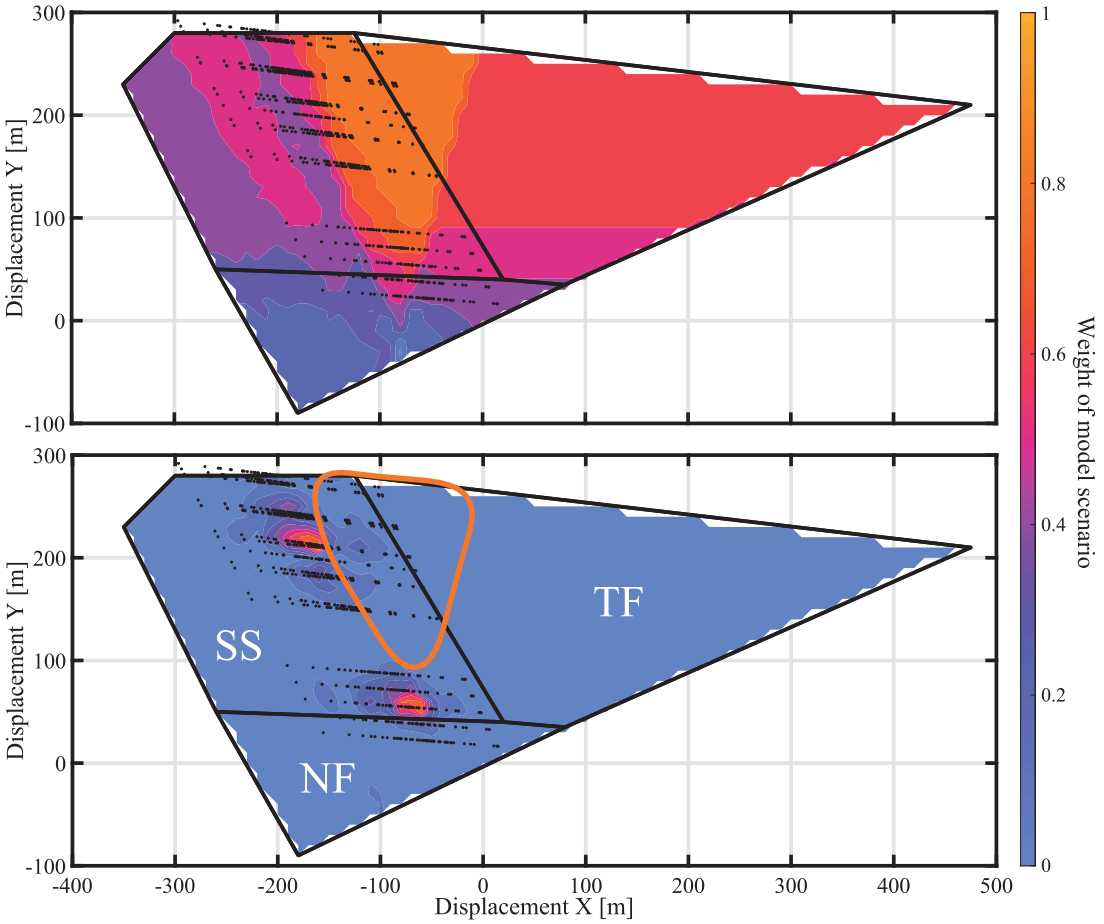

Figure 15. Comparison of the indirect weighting results only (top panel) with the Bayesian weighting results that include direct data on the stress magnitudes (bottom panel). Black dots are boundary conditions of model scenarios investigated by Ziegler & Heidbach (2023). Horizontal displacement boundary conditions with the highest probability according to indirect stress information (from the top) are shown in the bottom by the red-bordered polygon. Tectonic stress regimes indicated in the bottom part are the same for both parts.

presented in Ziegler & Heidbach (2020, 2023). The model covers a 140 × 70 × 11 km^3 part of the Bavarian Molasse Basin in Southern Germany around the city of Munich. In total, 13 lithologies are represented in the model by different rock properties. The original model uses 4 S_{Hmax} and 9 S_{hmin} stress magnitude data records to model likely data-supported stress states (Ziegler & Heidbach 2020). These stress states are weighted using a Bayesian approach based on indirect stress information from 55 FITs, 54 BOs, 5 DITFs, observed seismicity at 8 locations and explicitly observed seismic quiescence in 12 locations (Ziegler & Heidbach 2023).

In order to test the herein novel approach, the same Bayesian weighting approach with the same indirect stress information (P(C)) has been applied using the approach that is not limited to data-defined modelled stress states. Instead of weighting only those model scenarios that are based on available data records (Fig. 14a), model scenarios that comprise all possible stress states are evaluated (Fig. 14b). The weight of the stress data records (P(S)) is implemented as well and assigned to the according boundary conditions. Figs 14(c) and (d) show a comparison of the published results of Ziegler & Heidbach (2023) and the application of the new approach presented here. With the same data, the results of the weighting are almost identical. A slight difference can be observed due to an added prior probability for the tectonic stress regime (Fig. 14d). However, this is only observable for very small weights <0.1, that is very unlikely model scenarios. A significant impact of the regular grid in contrast to stress magnitude data-based model scenarios cannot be observed which indicates that the new approach can replace the previous one without reservation.

However, the entire strength of the new approach is not utilized by using it as a mere replacement of the previous approach. In particular, this holds for using a very strict weighting of P(S) founding on the stress magnitude data. In that case, the Bayesian weighting approach is bound to follow a possible bias introduced by the stress magnitude data. As presented, the result is very similar to the previous approach (Fig. 13). In that case, the only advantage is that of reducing the computation time to <1 per cent of the previous approach. A gain in information is not achieved this way. In order to take full advantage of the presented approach, the impact of P(S) in the Bayesian weighting scheme is significantly reduced or indirect stress information is regarded only. Fig. 15 shows a comparison of these two weighting approaches. The strength and benefit of the presented solution space-based approach are shown by two particular differences between the approaches—(1) the agreement between

indirect stress information and direct stress magnitude data and (2) a gain in information on the tectonic stress regime.

A comparison of Fig. 15 top and bottom shows that the boundary conditions of highest probability disagree. The stress magnitude data used for weighting (P(S)) are by far not representative for the most likely stress states based on indirect stress information. Instead, the stress magnitude data generally indicate too small magnitudes of S_{hmin} (approximately x-displacement). Only those S_{hmin} magnitudes considered outliers or extremely uncertain are actually within the area of highest agreement according to the indirect stress information (Fig. 15). A possible explanation for this offset can be found in the stress magnitude data that was used as prior probability (Ziegler & Heidbach 2023). In total, 9 S_{hmin} magnitude data records were available. Out of these, four data records are based on leak-off-tests (LOTs). In contrast to an extended LOT (XLOT) the informative value is clearly smaller, and an underestimation of the stress magnitude is more likely than in an XLOT or even a MHF test (Morawietz *et al.* 2020). Another four stress magnitude data records are based on estimations using the frictional equilibrium or stress polygon which is known to be based on many assumptions and thus its accuracy cannot compete with measurements (Morawietz *et al.* 2020). Finally, for one S_{hmin} data record no information about its type was available at all. This significantly decreases its value.

The S_{Hmax} magnitude data records, on the other hand, seem to be roughly in agreement with the S_{Hmax} magnitudes proposed by the indirect stress information (approximately y-displacement, Fig. 15). This comes as a surprise due to the notorious sparsity and unreliability of S_{Hmax} data records (Morawietz *et al.* 2020; Reiter *et al.* 2023; Ziegler & Heidbach 2023). However, this could be a misconception since no true and reliable upper limit exists for the y-displacement boundary conditions. If such constraints (Fig. 13) would be available, large portions of the most likely boundary conditions with large y-displacements might be ruled out.

The second significant difference concerns the present-day tectonic stress regime in the Bavarian Molasse Basin that is not clearly identified and described alternating as normal faulting, strike slip, or thrust faulting stress regime (Ziegler *et al.* 2016a and references therein). The stress magnitude data records often favour a strike slip stress regime (Fig. 14a) which is in agreement with seismological observations (Megies & Wassermann 2014, 2017). However, a normal faulting stress regime is also often postulated (Drews *et al.* 2019), while the prevalence of a thrust faulting stress regime is generally perceived as outdated. With strong P(S) weights, the preference for a strike slip stress regime with an option of a normal faulting stress regime is reflected in the results (Fig. 15 bottom). However, when only regarding the indirect stress information, a normal faulting stress regime can be ruled out with surprising certainty (Fig. 15 top). At the same time, the option for a thrust faulting stress regime, or at least a transtensional stress regime, becomes realistic (Fig. 15). The findings concerning the possibility of a thrust faulting stress regime are based on the agreement of indirect stress information with large x-displacements. Thus, they should be considered with care because they rely on few DITF data records and partly the sensitive and uncertain seismicity. Still, a new possibility emerged that would not have been identified without the herein presented approach.

In summary, the application of the new approach in the Bavarian Molasse Basin unearths some valuable new findings concerning the prevailing stress magnitudes and stress regime. This is only possible due to the unbiased nature of the approach and the inclusion of different data sources. Due to its speed and versatility the approach proves to be a valuable tool for the basin-wide assessment of the geomechanics.

5 CONCLUSION

State-of-the-art stress models face the challenge that the stress state is a result of subjective weighting of stress magnitude data and their large uncertainties which can furthermore include systematic errors. We developed an alternative approach that starts with an initially broad solution space which is narrowed down by simultaneously using stress magnitude data, tectonic stress regime estimates and indirect stress information such as FITs, BOs, DITFs and the occurrence of seismicity. This information is weighted using a Bayesian scheme in order to obtain a data-based model of the stress state that considers the uncertainties in all the stress data. In addition to an increase in objectivity the computational time is decreased to only a fraction of previous modelling approaches while shown to provide equivalent results. Furthermore, new findings of the area of interest in terms of the geomechanics are provided by the approach.

The presented research raises the question whether stress magnitude data are truly as important for the calibration of geomechanical models as they are often implied to be. In particular, since typically only few stress magnitude data records with variable quality are available where a single outlier has the potential to change the solution space in such a way that accuracy and precision are decreasing. In contrast, usage of indirect stress data has less potential to decrease the accuracy but at the same time does not provide a precision as high as it could be provided by a high-quality stress magnitude data record. In a trade-off, high accuracy is preferred as it determines the reliability of the median of predicted stress bandwidth. Thus, future research should investigate if the presented method is equivalent or even superior to using stress magnitude data records. In particular, in economic terms, not having to rely on expensive and often inaccurate stress magnitude data would be beneficial.

ACKNOWLEDGMENTS

The authors want to thank reviewers Sofie Gradmann and Dave Healy and editors Andrew Valentine, and Margarita Segou for their comments that helped to significantly improve the paper. Karsten Reiter and Tobias Hergert are acknowledged for comments on an early version of the paper. The work leading to these results has received funding from BGE SpannEnD 2.0, from the Federal Ministry for the Environment, Nature Conservation, Nuclear Safety and Consumer Protection through project SQuaRe (project number: 02E12062C), RI Fabrice Cotton and by the project PHYSALIS funded by the German Research Foundation (DFG grant 523456847).

AUTHOR CONTRIBUTION STATEMENT

MZ developed the used code and workflow and designed the study. OH assisted with study design and setup. Both authors contributed to the structure and writing of the paper.

DATA AVAILABILITY

The scripts used in the approach are publicly available (Ziegler & Heidbach 2021b; Ziegler 2023b) or on github.com/MorZieg and documented by (Ziegler & Heidbach 2021a; Ziegler 2023a).

REFERENCES

Aadnoy, B.S. & Bell, J.S., 1998. Classification of drilling-induced fractures and their relationship to in situ stress directions, *Log Analyst,* **39**(06), 27–42.

Ahlers, S. *et al.* 2022. The crustal stress field of Germany: a refined prediction, *Geotherm. Ener.,* **10**(1), doi:10.1186/s40517-022-00222-6.

Altmann, J.B., Müller, B.I.R., Müller, T.M., Heidbach, O., Tingay, M.R.P. & Weißhardt, A., 2014. Pore pressure stress coupling in 3D and consequences for reservoir stress states and fault reactivation, *Geothermics,* **52,** 195–205.

Amadei, B. & Stephansson, O., 1997. *Rock Stress and its Measurement,* Springer. doi: 10.1007/978-94-011-5346-1.

Baroň, I., Melichar, R., Sokol, Ľ., Rowberry, M., Plan, L. & Stemberk, J., 2024. 3D active fault kinematic behaviour reveals rapidly alternating near surface stress states in the Eastern Alps, *Geol. Soc., Lond., Spec. Publ.,* **546**(1), doi:10.1144/SP546-2023-32.

Barton, C.A., Zoback, M.D. & Burns, K.L., 1988. In-situ stress orientation and magnitude at the Fenton Geothermal Site, New Mexico, determined from wellbore breakouts, *Geophys. Res. Lett.,* **15**(5), 467–470.

Bell, J.S. & Gough, D.I., 1979. Northeast-southwest compressive stress in Alberta evidence from oil wells, *Earth planet. Sci. Lett.,* **45**(2), 475–482.

Brady, B.H.G. & Brown, E.T. 2006. *Rock mechanics for underground mining*. Springer Dordrecht. doi: 10.1007/978-1-4020-2116-9.

Cappa, F. & Rutqvist, J., 2012. Seismic rupture and ground accelerations induced by CO_2 injection in the shallow crust. *Geophys. J. Int.,* **190**(3), 1784–1789.

Desroches, J. *et al.* 2021. Stress measurement campaign in scientific deep boreholes: focus on tool and methods, in *Proceedings of the SPWLA 62nd Annual Online Symposium Transactions,* [Online].

Drews, M.C., Seithel, R., Savvatis, A., Kohl, T. & Stollhofen, H., 2019. A normal-faulting stress regime in the Bavarian Foreland Molasse Basin? New evidence from detailed analysis of leak-off and formation integrity tests in the greater Munich area, SE-Germany, *Tectonophysics,* **755,** 1–9.

Ellsworth, W.L., 2013. Injection-induced earthquakes, *Science,* **341**(6142), doi:10.1126/science.1225942.

Fischer, K. & Henk, A., 2013. A workflow for building and calibrating 3-D geomechanical models-a case study for a gas reservoir in the North German Basin, *Solid Earth,* **4**(2), 347–355.

Gaucher, E., Schoenball, M., Heidbach, O., Zang, A., Fokker, P., van Wees, J.-D. & Kohl, T., 2015. Induced Seismicity in Geothermal Reservoirs: A Review of ForecastingApproaches, *Renewable and Sustainable Energy Reviews,* **52,** 1473–1490.

Haimson, B.C. & Cornet, F.H., 2003. ISRM suggested methods for rock stress estimation-part 3: hydraulic fracturing (HF) and/or hydraulic testing of pre-existing fractures (HTPF), *Int. J. Rock Mech. Min. Sci.,* **40**(7–8), 1011–1020.

Hergert, T., Heidbach, O., Reiter, K., Giger, S.B. & Marschall, P., 2015. Stress field sensitivity analysis in a sedimentary sequence of the Alpine foreland, northern Switzerland, *Solid Earth,* **6**(2), 533–552.

Homberg, C., Hu, J.C., Angelier, J., Bergerat, F. & Lacombe, O., 1997. Characterization of stress perturbations near major fault zones: insights from 2-D distinct-element numerical modelling and field studies (Jura mountains), *J. Struct. Geol.,* **19**(5), 703–718.

Jaeger, J.C., Cook, N.G.W. & Zimmerman, R.W., 2007. *Fundamentals of Rock Mechanics,* 4th edn, Blackwell Publishing.

Kanamori, H., 1994. Mechanics of earthquakes, *Annu. Rev. Earth planet. Sci.,* **22,** 207–237.

Kirsch, E.G., 1898. *Die Theorie der Elastizität und die Bedürfnisse der Festigkeitslehre,* Zeitschrift Des Vereines Deutscher Ingenieure, 42pp.

Lecampion, B. & Lei, T., 2010. Reconstructing the 3D initial stress State over reservoir geomechanics model from local measurements and geological priors: a bayesian approach, *Schlumberger J. Model Des. Simul.,* **1,** 100–104.

Ljunggren, C., Chang, Y., Janson, T. & Christiansson, R., 2003. An overview of rock stress measurement methods, *Int. J. Rock Mech. Min. Sci.,* **40**(7–8), 975–989.

Mahmoodpour, S., Drews, M. & Duschl, F., 2023. Geomechanical forward modeling of the stress field, pore pressure and compaction in the North Alpine Thrust Front, SE Germany, in *EGU General Assembly 2023,* EGU23-7038, doi:10.5194/egusphere-egu23-7038.

Martínez-Garzón, P., Bohnhoff, M., Kwiatek, G. & Dresen, G., 2013. Stress tensor changes related to fluid injection at the Geysers geothermal field, California, *Geophys. Res. Lett.,* **40**(11), 2596–2601.

Martínez-Garzón, P., Kwiatek, G., Sone, H., Bohnhoff, M., Dresen, G. & Hartline, C., 2014. Spatiotemporal changes, faulting regimes, and source parameters of induced seismicity: a case study from the Geysers geothermal field, *J. geophys. Res.,* **119**(11), 8378–8396.

Megies, T. & Wassermann, J., 2014. Microseismicity observed at a non-pressure-stimulated geothermal power plant, *Geothermics,* **52,** 36–49.

Megies, T. & Wassermann, J., 2017. Mikroseismische aktivität geothermischer Systeme 2-vom einzelsystem zur groŷräumigen Nutzung Einzelprojekt 2-Untersuchungen zur optimierten seismischen überwachung hydrogeothermaler Systeme bei dichter räumlicher Lage der Bohrerlaubnisfelder am Beispiel der Situation im Süden Münchens.

Meier, T., Rybacki, E., Reinicke, A. & Dresen, G., 2013. Influence of borehole diameter on the formation of borehole breakouts in black shale, *Int. J. Rock Mech. Min. Sci.,* **62,** 74–85.

Meyer, H., Smith, J.D., Bourne, S. & Avouac, J.-P., 2023. An integrated framework for surface deformation modelling and induced seismicity forecasting due to reservoir operations, *Geol. Soc., Lond., Spec. Publ.,* **528**(1), 299–318.

Morawietz, S., Heidbach, O., Reiter, K., Ziegler, M.O., Rajabi, M., Zimmermann, G., Müller, B. & Tingay, M., 2020. An open-access stress magnitude database for Germany and adjacent regions, *Geotherm. Ener.,* **8**(1), doi:10.1186/s40517-020-00178-5.

Morris, A., Ferrill, D. & Brent, H., 1996. Slip-tendency analysis and fault reactivation. *Geology,* **24**(3), 275–278.

Müller, B., Schilling, F., Röckel, T. & Heidbach, O., 2018. Induced seismicity in reservoirs: stress makes the difference induzierte, *Erdöl Erdgas Kohle,* **1,** 33–37.

Plumb, R.A. & Hickman, S.H., 1985. Stress-induced borehole elongation: A comparison between the four-arm dipmeter and the borehole televiewer in the Auburn Geothermal Well *J. Geophys. Res.,* **90**(B7), 5513–5521.

Rahimi, R. & Nygaard, R., 2018. Effect of rock strength variation on the estimated borehole breakout using shear failure criteria, *Geomech. Geophys. Geo-Ener. Geo-Resour.,* **4**(4), 369–382.

Rajabi, M., Heidbach, O., Tingay, M. & Reiter, K., 2017. Prediction of the present-day stress field in the Australian continental crust using 3D geomechanical–numerical models, *Aust. J. Earth Sci.,* **64**(4), 435–454.

Rajabi, M., Tingay, M., King, R. & Heidbach, O., 2017. Present-day stress orientation in the Clarence-Moreton Basin of New South Wales, Australia: a new high density dataset reveals local stress rotations, *Basin Res.,* **29,** 622–640.

Reiter, K. & Heidbach, O., 2014. 3-D geomechanical-numerical model of the contemporary crustal stress state in the Alberta Basin (Canada), *Solid Earth,* **5**(2), 1123–1149.

Reiter, K., 2021. Stress rotation—impact and interaction of rock stiffness and faults, *Solid Earth,* **12**(6), 1287–1307.

Reiter, K., Heidbach, O., Ziegler, M., Giger, S., Garrard, R. & Desroches, J., 2023. Stress state estimation—new data and variability assessment of model results, *Saf. Nucl. Waste Dispos.,* **2,** 71–72.

Roche, V. & Van Der Baan, M., 2017. Modeling of the in situ state of stress in elastic layered rock subject to stress and strain-driven tectonic forces, *Solid Earth,* **8**(2), 479–498.

Rutqvist, J., Birkholzer, J.T. & Tsang, C.F., 2008. Coupled reservoir-geomechanical analysis of the potential for tensile and shear failure associated with CO2 injection in multilayered reservoir-caprock systems, *Int. J. Rock Mech. Min. Sci.,* **45**(2), 132–143.

Schmitt, D.R., Currie, C.A. & Zhang, L., 2012. Crustal stress determination from boreholes and rock cores: fundamental principles, *Tectonophysics,* **580,** 1–26.

Schoenball, M., Walsh, F.R., Weingarten, M. & Ellsworth, W.L., 2018. How faults wake up: the Guthrie-Langston, Oklahoma earthquakes, *Leading Edge,* **37**(2), 100–106.

Segall, P. & Fitzgerald, S., 1998. A note on induced stress changes in hydrocarbon and geothermal reservoirs, *Tectonophysics,* **289**(1–3), 117–128.

Shatyrbayeva, I., Bohnsack, D., Duschl, F. & Drews, M.C., 2023. Comparison and integration of pore pressure measurements and indicators from drilling data in a deep geothermal energy play in SE Germany, *Geoenergy,* **1**(1), doi:10.1144/geoenergy2023-038.

Townend, J. & Zoback, M.D., 2000. How faulting keeps the crust strong, *Geology,* **28**(5), 399–402.

Vernik, L. & Zoback, M.D., 1992. Estimation of maximum horizontal principal stress magnitude from stress-induced well bore breakouts in the Cajon Pass scientific research borehole, *J. geophys. Res.,* **97**(B4), 5109–5119.

van Wees, J.-D., Osinga, S., Van Thienen-Visser, K. & Fokker, P.A., 2018. Reservoir creep and induced seismicity: Inferences from geomechanical modeling of gas depletion in the Groningen field, *Geophys. J. Int.,* **212**(3), 1487–1497.

Wileveau, Y., Cornet, F.H., Desroches, J. & Blumling, P., 2007. Complete in situ stress determination in an Argillite sedimentary formation, *Phys. Chem. Earth, Parts A/B/C,* **32**(8–14), 866–878.

Zang, A. & Stephansson, O., 2010. *Stress Field of the Earth's Crust,* Springer. doi: 10.1007/978-1-4020-8444-7.

Ziebarth, M., von Specht, S., Heidbach, O., Cotton, F. & Anderson, J.G., 2020. Applying Conservation of Energy to Estimate Earthquake Frequencies from Strain Rates and Stresses, *J. Geophys. Res.: Solid Earth,* **125,** e2020JB020186. doi: 10.1029/2020JB020186.

Ziegler, M., Reiter, K., Heidbach, O., Zang, A., Kwiatek, G., Stromeyer, D., Dahm, T., Dresen, G. & Hofmann, G., 2015. Mining-Induced Stress Transfer and Its Relation to a 1.9 Seismic Event in an Ultra-deep South African Gold Mine, *Pure Appl. Geophys.,* **172,** 2557–2570.

Ziegler, M.O. & Heidbach, O., 2020. The 3D stress state from geomechanical–numerical modelling and its uncertainties: a case study in the Bavarian Molasse Basin, *Geotherm. Ener.,* **8,** doi:10.1186/s40517-020-00162-z.

Ziegler, M.O. & Heidbach, O., 2021a. Manual of the Python script PyFAST calibration v1.0. https://doi.org/10.48440/wsm.2021.003.

Ziegler, M.O. & Heidbach, O., 2021b. Python script PyFAST calibration v.1.0 (V.1.0). GFZ Data Services. http://doi.org/10.5880/wsm.2021.003.

Ziegler, M.O. & Heidbach, O., 2023. Bayesian quantification and reduction of uncertainties in 3D geomechanical-numerical models, *J. geophys. Res.,* **128**(1), doi:10.1029/2022JB024855.

Ziegler, M.O., 2023a. Manual of the Python script FAST Estimation v1.0. https://doi.org/10.48440/wsm.2023.001.

Ziegler, M.O., 2023b. Python script FAST estimation v.1.0 (V.1.0), GFZ Data Services. http://doi.org/10.5880/wsm.2023.001.

Ziegler, M.O., Heidbach, O., Morawietz, S. & Wang, Y., 2023. Manual of the Matlab Script FAST Calibration v2.4. https://doi.org/10.48440/wsm.2023.002.

Ziegler, M.O., Heidbach, O., Reinecker, J., Przybycin, A.M. & Scheck-Wenderoth, M., 2016a. Corrigendum to "A multi-stage 3-D stress field modelling approach exemplified in the Bavarian Molasse Basin", *Solid Earth,* **7,** 1365–1382.

Ziegler, M.O., Heidbach, O., Reinecker, J., Przybycin, A.M. & Scheck-Wenderoth, M., 2016b. A multi-stage 3-D stress field modelling approach exemplified in the Bavarian Molasse Basin, *Solid Earth,* **7**(5), 1365–1382.

Ziegler, M.O., Heidbach, O., Zang, A., Martínez-Garzón, P. & Bohnhoff, M., 2017. Estimation of the differential stress from the stress rotation angle in low permeable rock, *Geophys. Res. Lett.,* **44**(13), 6761–6770.